Quantification of Vortex Flow in Pulmonary Arteries of Patients With Chronic Thromboembolic Pulmonary Hypertension

Hiroki Kamada (hkamada@rad.med.tohoku.ac.jp)
Tohoku University Hospital: Tohoku Daigaku Byoin https://orcid.org/0000-0003-3341-9396
Hideki Ota
Tohoku University Hospital: Tohoku Daigaku Byoin
Masanori Nakamura
Nagoya Institute of Technology Electrical and Mechanical Engineering: Nagoya Kogyo Daigaku Denki Kikai Kogakuka Denki Kikai Kogaku Kenkyuka
Wenyu Sun
Tohoku University Hospital: Tohoku Daigaku Byoin
Tatsuo Aoki
Tohoku University: Tohoku Daigaku
Haruka Sato
Tohoku University: Tohoku Daigaku
Koichiro Sugimura
Tohoku University: Tohoku Daigaku
Kei Takase
Tohoku University Hospital: Tohoku Daigaku Byoin

Research Article

Keywords: 4D-flow MRI, CTEPH, BPA, blood flow

Posted Date: April 21st, 2021

DOI: https://doi.org/10.21203/rs.3.rs-436343/v1

Version of Record: A version of this preprint was published at European Journal of Radiology on January 1st, 2022. See the published version at https://doi.org/10.1016/j.ejrad.2021.110142.

Quantification of vortex flow in pulmonary arteries of patients with chronic thromboembolic pulmonary hypertension

Purpose: This study proposes an objective method of quantifying the vortex flow in pulmonary arteries to compare the duration of its presence before and after balloon pulmonary angioplasty (BPA) in patients with chronic thromboembolic pulmonary hypertension (CTEPH).

Methods: Thoracic 4D-flow magnetic resonance imaging was performed in 28 CTEPH patients before and after BPA. Planes were set in pulmonary arteries to evaluate volume flow rate (VFR), the duration, and area of backward flow in the pulmonary trunk, which is a component of the vortex flow. The full width at half maximum (FWHM) of the peak of the time course of VFR of backward flow was assessed to quantify the duration of the vortical flow.

Results: Although overall flow patterns after BPA appeared to be the same as the one before BPA, significant decreases in the FWHM, area, and VFR of the backward flow after BPA were found (FWHM: before, $1.88\times10^{-1} \pm 1.51\times10^{-2}$ [cardiac cycle] vs. after,

$1.65\times10^{-1} \pm 1.86\times10^{-2}$ [cardiac cycle]; area ratio: before, $2.67\times10^{-1} \pm 1.30\times10^{-2}$ vs. after, $2.38\times10^{-1} \pm 1.31\times10^{-2}$; VFR: before, 13.6±2.21 [mL/s] vs. after, 11.3±2.36 [mL/s]).

Conclusion: BPA promoted significant decreases in the FWHM, area, and VFR of backward flow in the pulmonary trunk, thereby facilitating efficient blood transport. The tendencies for these changes were to be larger for cases where BPA more greatly decreased the pressure. The results suggest that the FWHM, area, and VFR are useful indicators for the noninvasive evaluation of the therapeutic effects of BPA.

Key words

4D-flow MRI; CTEPH; BPA; blood flow

Abbreviations

Chronic thromboembolic pulmonary hypertension (CTEPH)

Pulmonary artery pressure (PAP)

Right heart catheterization (RHC)

Balloon pulmonary angioplasty (BPA)

Magnetic resonance (MR) imaging

Three-dimensional phase-contrast magnetic resonance imaging (4D-flow MRI)

Volume flow rate (VFR)

Electrocardiogram (ECG)

Pulmonary vascular resistance (PVR)

Right ventricular ejection fraction (RVEF)

Right ventricular cardiac index (RVCI)

Velocity encoding (VENC)

Full width at half maximum (FWHM)

Flow momentum index (FMI)

Reynolds number (Re)

Transtricuspid pressure gradient (TRPG)

Introduction

Chronic thromboembolic pulmonary hypertension (CTEPH) is characterized by the presence of organized thrombi in the pulmonary arteries (PAs) [1]. Without appropriate treatment, CTEPH has poor prognosis due to progressive right ventricular heart failure [2]. Mean PA pressure (PAP) measured via right heart catheterization (RHC) is an important metric in the diagnosis, prognosis, and response to therapy of this condition. Pulmonary endarterectomy has been the standard treatment for CTEPH. However, it is not suitable for patients whose arteriopathy is located in the distal vessels [3]. In this regard, balloon pulmonary angioplasty (BPA) may be an alternative treatment for patients with distal-type CTEPH or those not suited to surgery [4,5].

Time-resolved, three-dimensional (3D), phase-contrast, magnetic resonance imaging (4D-flow MRI) has been applied to analyze blood flow in the heart and large vessels [6]. Its use allows not only the visualization of flow patterns but also analyses of various fluid mechanical quantities, such as vorticity, helicity, and wall shear stress [7,8,9].

Previous studies have implicated vortex flow in the PA as an abnormal blood flow for patients with pulmonary hypertension [7,10,11]. Reiter et al. evaluated the relative duration of the vortical flow in a cardiac cycle by viewing velocity fields and

68 reported a strong correlation between the duration of vortical blood flow in the main PA
69 and mean PAP in patients with pulmonary hypertension [10]. This result strongly
70 suggests that vortical flow can be used as a marker of pulmonary hypertension.
71 However, visual assessment of blood flow is difficult, particularly when it has a
72 complex structure and variable momentum, and thus such assessment is prone to be
73 subjectivity and being dependent on the observer. In Reiter et al. (2014)[10], the
74 assessment was done by two readers with 12 years of experience in cardiac MRI. In
75 addition, visual assessment of blood flow with a complex 3D structure is
76 time-consuming because such a structure appears different depending on the viewing
77 angle; reportedly, the visual assessment of the vortical flow took between 15 and 25 min
78 per patient [10]. Therefore, a quantitative, objective evaluation of the vortex flow in the
79 PA that requires less effort is necessary for clinical application, such as evaluation of the
80 therapeutic effects and long-term monitoring of pulmonary hypertension.

81 In this study, we propose a more objective way of quantifying the vortical flow
82 in the PA with a focus on the backward flow component, a part of the vortex flow. The
83 duration, volume flow rate (VFR), and cross-sectional area of the backward flow was
84 evaluated from time-resolved, 3D velocity fields obtained by 4D-flow MRI. We also
85 assessed the structure of blood flow using various fluid mechanical indices that

represent the flow complexity. The hemodynamics in the PA before and after BPA in patients with CTEPH were compared to assess the efficacy of the proposed method.

Methods

Study population

This study was approved by the local institutional review board and written informed consent was obtained for each patient. In all, 28 CTEPH patients (7 men and 21 women; mean age, 68 years; range, 50–83 years) were prospectively enrolled. Based on the National Institute for Health and Care Excellence criteria [12], all patients were diagnosed with CTEPH by medical history, physical examination, electrocardiogram (ECG), chest X-ray, echocardiography, lung ventilation/perfusion scintigraphy, RHC, and computed tomography angiography or PA angiography. The patients were treated with the optimal medical therapy and several sessions of BPA (mean, 3.7 ± 0.29). In one procedure, the target lesion was limited to 1 or 2 segments in one lobe to minimize the complications from BPA. The sessions of BPA were repeated until the mean PAP became less than 30 [mmHg] at a 4–8 week interval [13]. RHC after interventions showed decreases in mean PAP (before, 40 ± 1.6 [mmHg] vs. after, 25 ± 1.3 [mmHg]). The postoperative pressure decrease in mean PAP (ΔP) was 15 ± 1.6 [mmHg] (range, 3-28 [mmHg]; median, 14 [mmHg]). RHC data before and after BPA is summarized in Table 1. No patients manifested a severe complication, however, some patients had blood sputum and mild or moderate hemoptysis; they were treated noninvasively.

Thoracic 4D-flow MRI

Thoracic 4D-flow MRI examinations were performed in patients before and after sessions of BPA (mean interval, 363 ± 29.6 [days]) using a 3.0 T scanner (MAGNETOM Trio, A Tim System; Siemens Healthineers, Enlargen, Germany). The MRI was performed with the following parameters: 3D phase-contrast MRI with three-directional velocity encoding transverse acquisition; ECG gating; respiratory gating; TR/TE, 42.6/2.54 [ms]; flip angle, 15 [°]; velocity encoding (VENC), 70 [cm/s], spatial resolution, 2.4 × 1.8 × 3.5 [mm^3]; time resolution, 14–24 [phases/cardiac cycle].

Quantification of blood flow and vessel geometry

Prototype post-processing software (4D-flow Demonstrator version 2.3; Siemens Healthineers, Enlargen, Germany) was used to visualize the cardiovascular geometry and blood flow patterns. Cross-sectional planes were set at the inlets of the pulmonary trunk, right, and left main PAs to evaluate VFR, as shown in Fig. 1. In addition, 30 planes were set in the pulmonary trunk along the centerline to evaluate net VFR and secondary flow in each plane.

The duration of the vortical flow (the length of cardiac phases with vortex

126 present) was quantified as the full width at half maximum (FWHM) of the peak of the
127 time course of VFR of backward flow (VFR), as depicted in Fig. 1. The FWHM does
128 not exactly represent the duration of vortex flow but dose quantify the length of time
129 that vortex flow exists with a high momentum, which is considered to have a relatively
130 large impact on pulmonary blood flow during a cardiac cycle.

131 The size of vortical flow was evaluated as the proportion of the area of the
132 backward flow present in each cross-section, and the time-averaged area ratio was
133 defined by

134 $$\overline{\text{area ratio}} = \sum^{N_\text{p}} A_\text{b}/A \Big/ N_\text{p} \quad (1)$$

135 where A_b is the cross-sectional area occupied by the backward flow, A is the entire
136 cross-sectional area, and N_p is the number of data acquisition phases of 4D-MRI (i.e.,
137 time resolution 14–24 phases/cardiac cycle).

138 The velocity, $\boldsymbol{v}$, in a cross-sectional plane may be either forward or backward
139 ($v_{\text{n,f}}$ and $v_{\text{n,b}}$), as shown in Fig. 1. The mean backward flow rate during a cardiac cycle is

140 $$\overline{\text{VFR}_\text{b}} = \sum^{N_\text{p}} \text{VFR}_\text{b} \Big/ N_\text{p} = \sum^{N_\text{p}} \int |\boldsymbol{v}_{n,\text{b}}| A_\text{b} \Big/ N_\text{p} \quad (2)$$

141 where $v_{\text{n,b}}$ is the normal component of the spatially averaged backward flow velocity.

142 The laminar-to-turbulent nature of the blood flow was assessed with the
143 Reynolds number (Re) defined as

$$\mathrm{Re} = {}^{uD}/_{\nu} \quad (3)$$

where u is a representative velocity, D is the diameter of the blood vessel, and ν is the kinematic viscosity. The normal component of the spatially averaged velocity in a cross-sectional plane was used as the representative velocity. The kinetic viscosity of blood was approximated by $\nu = 3.3 \times 10^{-6}$ [m^{2}/s].

Flow complexity was assessed with various fluid mechanical indices, namely, the flow momentum index (FMI), enstrophy density, and helicity density (H_d). The FMI represents the relative strength of secondary flow [14] and is defined as the ratio between the norms of the in-plane and a cross-sectional plane components of velocity ($|v_s|$ and $|v|$, respectively). Enstrophy density describes the strength of vorticity and is defined as one half of the square of the vorticity [15]. H_d indicates the strength and direction of rotation of the vorticity at a position and is defined as the inner product of the velocity and vorticity [9].

The vortex structure of blood flow was characterized with the second invariant of the velocity gradient tensor (Q) [16]. A region with positive Q-value represents the existence of a vortex core, and thus Q value was evaluated to visualize the vortex structure.

The geometric features of the PA, such as diameter, curvature, and bifurcation

angle, were assessed. The mean diameter of the pulmonary trunk was calculated as time-averaged mean diameter in the 30 planes. The vessel curvature is the reciprocal of the radius of curvature that is equal to a circumradius of the triangle formed by a point on the centerline and two neighboring points. 30 points were set in the centerline of the pulmonary trunk, and the mean curvature was defined as the average of curvatures at each point. The bifurcation angle was defined as the angle between the center of the outlet of the pulmonary trunk and those of inlets of the right and left main PAs.

We assessed the parameters before and after BPA and explored the relationship between the parameters and mean PAP obtained by RHC. The parameters were calculated using in-house codes implemented with MATLAB 2018b software (MathWorks, Natick, *Massachusetts*, USA). Data smoothing for velocity fields was done with a 3 × 3 × 3 median filter and 3D Gaussian filter ($\sigma = 0.5$).

Statistical analyses

Statistical parameters, such as the mean value, range, standard deviation, standard error, and paired t-test results, were calculated using JMP pro version 14 software (SAS Institute, Cary, North Carolina, USA). A *p*-value of less than 0.05 was considered to be statistically significant.

180

181

Results

Volume flow rate and duration of backward flow in the main pulmonary artery

Figure 2 shows the FWHM, the area ratio, and $\overline{\mathrm{VFR_b}}$ in the pulmonary trunk. The values are the means obtained for the 30 cross-sectional planes in the pulmonary trunk. Compared to their values before BPA, the FWHM, the area ratio, and $\overline{\mathrm{VFR_b}}$ after BPA all significantly changed: the FWHM shortened (before, $1.88 \times 10^{-1} \pm 1.51 \times 10^{-2}$ [cardiac cycle] vs. after, $1.65 \times 10^{-1} \pm 1.86 \times 10^{-2}$ [cardiac cycle], $p = 0.0429$), the area ratio decreased (before, $2.67 \times 10^{-1} \pm 1.30 \times 10^{-2}$ vs. after, $2.38 \times 10^{-1} \pm 1.31 \times 10^{-2}$, $p = 0.0034$), and the $\overline{\mathrm{VFR_b}}$ decreased (before, 13.6 ± 2.21 [mL/s] vs. after, 11.3 ± 2.36 [mL/s], $p = 0.009$). The values of the perioperative ratios of FWHM ($=\mathrm{FWHM_{after}/FWHM_{before}}$), area ratio ($=(A_b/A)_{after}/(A_b/A)_{before}$), and $\overline{\mathrm{VFR_b}}$ ($=\overline{\mathrm{VFR_{b,after}}}/\overline{\mathrm{VFR_{b,before}}}$) were 0.88 ± 0.053, 0.91 ± 0.039 and 0.91 ± 0.099, respectively. There were no statistical correlations between ΔP and FWHM, area ratio, or $\overline{\mathrm{VFR_b}}$.

We classified the cases into two groups with reference to the median ΔP of 14 [mmHg]: the large (ΔP ≥ 14 [mmHg], 15 cases) and small (ΔP < 14 [mmHg], 13 cases) decrease groups. The mean PAPs before BPA were 45 ± 1.6 [mmHg] and 35 ± 2.3 [mmHg] for the large and small decrease groups, respectively. The values after BPA

were 23 ± 1.6 [mmHg] and 28 ± 2.0 [mmHg]. Figure 3 shows the FWHW, area ratio, and $\overline{VFR_b}$ for the two groups. All of the parameters significantly decreased in the large decrease group (FWHM: before, $1.79 \times 10^{-1} \pm 1.61 \times 10^{-2}$ [cardiac cycle] vs. after, $1.44 \times 10^{-1} \pm 1.54 \times 10^{-2}$ [cardiac cycle], $p = 0.0064$; area ratio: before, $2.63 \times 10^{-1} \pm 1.27 \times 10^{-2}$ vs. after, $2.25 \times 10^{-1} \pm 1.08 \times 10^{-2}$, $p = 0.0058$; $\overline{VFR_b}$: before, 11.7 ± 1.56 [mL/s] vs. after, 7.9 ± 9.99 [mL/s], $p = 0.0097$). On the other hand, no statistically significant postoperative differences were noted in the small decrease group (FWHM: before, $1.98 \times 10^{-1} \pm 2.72 \times 10^{-2}$ [cardiac cycle] vs. after, $1.90 \times 10^{-1} \pm 3.56 \times 10^{-2}$ [cardiac cycle], $p = 0.328$; area ratio: before, $2.72 \times 10^{-1} \pm 2.46 \times 10^{-2}$ vs. after, $2.52 \times 10^{-1} \pm 2.53 \times 10^{-2}$, $p = 0.114$; $\overline{VFR_b}$: before, 15.7 ± 4.43 [mL/s] vs. after, 15.1 ± 4.64 [mL/s], $p = 0.373$).

Volume flow rate at the inlets of the pulmonary trunk and bilateral main pulmonary artery

Figure 4 shows the time-averaged VFR ($\overline{VFR}$) at the inlet of the pulmonary trunk. As the perioperative ratio was 1.34 ± 0.186, a statistically significant increase in the $\overline{VFR}$ after BPA was discovered (before, 72.5 ± 4.15 [mL/s] vs. after, 84.5 ± 4.33 [mL/s], $p = 0.0148$). $\overline{VFR}$s increased at the inlets of the bilateral main PAs (right: before, 10.6 ± 1.56 [mL/s] vs. after, 14.4 ± 2.07 [mL/s], $p = 0.0428$; left: before, 13.2 ± 1.79 [mL/s] vs.

after, 13.9 ± 1.91 [mL/s], p = 0.341). The split ratio of the flow between the right and left main PAs (=$\overline{\mathrm{VFR}_{\mathrm{right}}}/(\overline{\mathrm{VFR}_{\mathrm{right}}} + \overline{\mathrm{VFR}_{\mathrm{left}}})$) did not significantly change (before, 43 ± 5.75% vs. after, 49 ± 5.29%, p = 0.262).

The $\overline{\mathrm{VFR}}$ at the inlet of the pulmonary trunk significantly increased in the large decrease group (before, 67.6 ± 5.57 [mL/s] vs. after, 85.4 ± 6.55 [mL/s], p = 0.0173), whereas no significant change was observed in the small decrease group (before, 78.2 ± 6.08 [mL/s] vs. after, 83.4 ± 5.73 [mL/s], p = 0.118). The perioperative ratios were 1.54 ± 0.34 and 1.13 ± 0.086 in the large and small decrease groups, respectively.

Blood flow structure and flow complexity

Figure 5 shows representative streamlines in late systole of two patients; one is in the large decrease group whose mean PAP decreased from 48 to 20 [mmHg], and the other is in the small decrease group whose mean PAP decreased from 47 to 40 [mmHg]. The streamlines are colored according to the value of the streamwise velocity. The perioperative changes in the streamlines did not show any notable difference between the two cases. Before BPA, the flow was disturbed with vortices in the PAs (Fig. 5A and C). Afterward, the flow disturbance in late systole was attenuated and streamwise

236 velocity increased, although a vortical flow was still present in the pulmonary trunk (Fig.
237 5B and D).

238 Figure 6 shows isosurface plots of H_d and Q-value during late systole in those
239 same two patients as displayed in Fig. 5. The sign of H_d changes according to the
240 directions of the velocity and vorticity, with red (blue) indicating positive (negative)
241 values of H_d. Regions of positive and negative H_d can be seen in the pulmonary trunk,
242 indicating that local blood flow was spinning in different directions. Considering the
243 perioperative change in distribution of positive and negative H_d regions, no notable
244 differences between the two cases were noted. Before BPA, positive and negative H_d
245 regions were observed in the pulmonary trunk (Fig. 6A and C, left). Even after BPA,
246 positive and negative H_d regions were still observed, suggesting the existence of helical
247 flow (Fig. 6B and D, left).

248 The region of positive Q-value indicates the existence of a vortex core.
249 Likewise, there was no notable difference between the two cases, in terms of the
250 perioperative change in the distribution of the positive Q-value region (the large
251 decrease group, Fig. 6A and B, right; the small decrease group, Fig. 6C and D, right).

252 Neither FMI nor enstrophy density for all patients showed significant changes
253 with BPA (FMI: before, 0.609 ± 0.0128 vs. after, 0.594 ± 0.0122, $p = 0.917$; enstrophy

density: before, $2.71 \times 10^4 \pm 1.90 \times 10^3$ [$1/s^2$] vs. after, $2.95 \times 10^4 \pm 3.94 \times 10^3$ [$1/s^2$], $p = 0.196$).

Reynolds number (Re) and vessel geometry

After BPA, peak and mean Re significantly increased (peak: before, 3580 ± 158 vs. after, 4120 ± 214, $p = 0.0098$; mean: before, 888 ± 49.5 vs. after, 1110 ± 60.8, $p = 0.0007$).

The diameter of the pulmonary trunk significantly decreased (before, 34.8 ± 0.879 [mm] vs. after, 33.4 ± 0.828 [mm], $p = 0.0009$). The mean curvature of the pulmonary trunk and bifurcation angle did not show any significant change (mean curvature: before, 35.5 ± 2.8 [m^{-1}], vs after, 33.3 ± 2.1 [m^{-1}], $p = 0.47$; bifurcation angle: before, 83 ± 2.3 [°] vs after, 84 ± 2.2 [°], $p = 0.59$).

Discussion

The major findings of the present study are two-folds. First, for the backward flow in the pulmonary trunk, its duration, extent of its region, and its VFR all significantly decreased after BPA. Second, the fluid mechanical indices representing the complexity of blood flow did not show a significant change after BPA, despite an increase in Re (i.e., the blood flow may now be disturbed more easily).

Perioperative changes in backward flow and whole pulmonary blood flow

A postoperative decrease in mean PAP by RHC is a major therapeutic effect [5,17,18]. Pressure and velocity are closely associated in blood flow, and the pressure gradient can be calculated from the velocity field using fluid mechanics. However, it is not possible to calculate the absolute blood pressure solely from a velocity field. Previous studies have investigated the relationship between mean PAP and velocity field [7,19,20,21]. Reiter et al. (2015)[10] observed vortices in the pulmonary trunk for patients with pulmonary hypertension, and successfully demonstrated a strong correlation between appearance time of vortices and mean PAP. Using the same technique, Ramos et al. (2020)[21] demonstrated a correlation between mean PAP, estimated by the duration, and the transtricuspid pressure gradient (TRPG). Because vortical flow in the PA has a

3D structure and coexists with helical flow, it is difficult to accurately make a visual assessment of changes in its size and duration. Therefore, a quantitative and objective way to assess it is desired. For backward flow, the present results show decreases in FWHM, extent of the region, and VFR after BPA. These changes were larger in cases with larger pressure decreases. Therefore, these factors are useful indicators for noninvasive evaluation of the therapeutic effects of BPA.

Perioperative changes in the complexity of blood flow

A flow pattern and its complexity are determined by vessel geometry and flow rate. In terms of vessel geometry, the curvature from the pulmonary trunk and the bifurcation angle did not show any significant change from BPA, while the vessel diameter decreased. In fluid mechanics, Re is a key index to represent the nature of a flow, i.e., laminar or turbulent. In the present study, the mean Re increased, up to ~1100, after BPA. This implies that the blood flow is still laminar, but a flow with a larger Re can be disturbed more easily than the one with a smaller value [22]. Notwithstanding an increase in Re, the streamlines after BPA demonstrate regression of the flow disturbance. Moreover, the fluid mechanical indices that describe flow complexity, such as FMI and

304 enstrophy density, did not show any significant changes after BPA. These perioperative
305 changes indicate that blood transport in the pulmonary trunk is facilitated by BPA.
306
307 **Limitations**
308 There were some limitations to this study. First, the VFR at the inlet of the pulmonary
309 trunk did not coincide with the sum of those at the inlets of the bilateral PAs, as shown
310 in Fig. 4. There are two factors associated with the inaccuracy of phase-contrast MRI:
311 the VENC setting and the flow-related dephasing in phase-contrast MRI. Concerinng
312 the former, the VENC might be set high to cope with the high velocity of the blood flow,
313 thus reducing the velocity sensitivity for any relatively slow flow. In the latter,
314 dephasing due to a disturbed flow can cause signal loss [23]. Second, the number of
315 patients was relatively small. Third, the follow-up 4D-flow MRI was performed only
316 once after BPA. After BPA, right ventricular reverse remodeling has been reported [17];
317 this would be associated with a change in the cardiovascular outcome in patients with
318 CTEPH. A long-term follow-up study could detect any additional changes in the PA
319 blood flow.
320
321 **Conclusions**

We developed an objective method of quantifying the vortex flow in the PA, focusing on backward flow as a component of this vortex flow. This thoracic 4D-flow MRI study of patients with CTEPH quantitatively demonstrated that the FWHM, the area ratio, and VFR of the backward flow in the pulmonary trunk significantly decreased after BPA. These changes tended to be larger in cases where ΔP was larger. These results suggest that these factors are useful indicators for noninvasive evaluation of the therapeutic effects of BPA.

Acknowledgement

The authors are grateful to Tatsuo Nagasaka and Tomoyoshi Kimura for support with 4D-flow MRI scan, Shin Chibana for his support with post processing of image data, Aurelien F. Stalder (Siemens Healthineer GmbH) for providing 4D-Flow Demonstrator, and Yoshiaki Komori and Yuta Urushibata (Siemens Healthcare K.K.) for support with acquisition of 4D-flow MRI.

Declarations

Conflict of interest

The authors have no conflict of interest to declare.

Ethical approval

The present study was approved by the ethics committee of Tohoku University (2014-1-875).

References

1. D'Armini AM. Diagnostic advances and opportunities in chronic thromboembolic pulmonary hypertension. Eur Respir Rev 2015;24(136):253-262. doi:10.1183/16000617.00000915

2. Dentali F, Donadini M, Gianni M, et al. Incidence of chronic pulmonary hypertension in patients with previous pulmonary embolism. Thromb Res 2009;124(3):256-258. doi:10.1016/j.thromres.2009.01.003

3. Yamada N. Beneficial Therapeutic Effects of Balloon Pulmonary Angioplasty on Biventricular Function in Patients With Chronic Thromboembolic Pulmonary Hypertension. Circ J 2016;80(6):1326-1327. doi:10.1253/circj.CJ-16-0418

4. Gopalan D, Delcroix M, Held M. Diagnosis of chronic thromboembolic pulmonary hypertension. Eur Respir Rev 2017;26(143):160108. Published 2017 Mar 15. doi:10.1183/16000617.0108-2016

5. Aoki T, Sugimura K, Tatebe S, et al. Comprehensive evaluation of the effectiveness and safety of balloon pulmonary angioplasty for inoperable chronic thrombo-embolic pulmonary hypertension: long-term effects and procedure-related complications. Eur Heart J 2017;38:3152–9.

6. Markl M, Frydrychowicz A, Kozerke S, et al. 4D flow MRI. J Magn Reson

Imaging 2012;36(5):1015-1036. doi:10.1002/jmri.23632.

7. Barker AJ, Roldán-Alzate A, Entezari P, et al. Four-dimensional flow assessment of pulmonary artery flow and wall shear stress in adult pulmonary arterial hypertension: results from two institutions. Magn Reson Med 2015;73(5):1904-1913. doi:10.1002/mrm.25326

8. Schäfer M, Barker AJ, Kheyfets V, et al. Helicity and Vorticity of Pulmonary Arterial Flow in Patients With Pulmonary Hypertension: Quantitative Analysis of Flow Formations. J Am Heart Assoc 2017;6(12):e007010. Published 2017 Dec 20. doi:10.1161/JAHA.117.007010

9. Kamada H, Ota H, Nakamura M, et al. Perioperative Hemodynamic Changes in the Thoracic Aorta in Patients With Aortic Valve Stenosis: A Prospective Serial 4D-Flow MRI Study. Semin Thorac Cardiovasc Surg 2020;32(1):25-34. doi:10.1053/j.semtcvs.2019.07.006

10. Reiter G, Reiter U, Kovacs G, et al. Blood flow vortices along the main pulmonary artery measured with MR imaging for diagnosis of pulmonary hypertension. Radiology 2015;275(1):71-79. doi:10.1148/radiol.14140849

11. Ota H, Sugimura K, Miura M et al. Four-dimensional flow magnetic resonance imaging visualizes drastic change in vortex flow in the main pulmonary artery after

384 percutaneous transluminal pulmonary angioplasty in a patient with chronic
385 thromboembolic pulmonary hypertension. Eur Heart J 2015;36(25):1630.
386 doi:10.1093/eurheartj/ehv054
387 12. Galiè N, Humbert M, Vachiery JL, et al. 2015 ESC/ERS Guidelines for the
388 diagnosis and treatment of pulmonary hypertension: The Joint Task Force for the
389 Diagnosis and Treatment of Pulmonary Hypertension of the European Society of
390 Cardiology (ESC) and the European Respiratory Society (ERS): Endorsed by:
391 Association for European Paediatric and Congenital Cardiology (AEPC),
392 International Society for Heart and Lung Transplantation (ISHLT). Eur Heart J
393 2016;37(1):67-119.
394 13. Sugimura K, Fukumoto Y, Satoh K, et al. Percutaneous transluminal pulmonary
395 angioplasty markedly improves pulmonary hemodynamics and long-term
396 prognosis in patients with chronic thromboembolic pulmonary hypertension. Circ J
397 2012;76(2):485-488. doi:10.1253/circj.cj-11-1217
398 14. Nakamura M, Wada S, Yamaguchi T. Quantitative evaluation of intra-aortic flow
399 disturbance by the fluid momentum index: Effect of the left ventricular systolic
400 function on the hemodynamics in the aorta. Technol Health Care 2007;15(2):111-
401 120.

15. Miura H, Enstrophy generation in a shock-dominated turbulence. J Phys Soc Jpn 1996;65(2):450-461. doi.org/10.1143/jpsj.65.450

16. Chen Q, Zhong Q, Meilan Qi, et al. Comparison of vortex identification criteria for planar velocity fields in wall turbulence. Phis Fluids 2015;27:085101.

17. Fukui S, Ogo T, Morita Y, et al. Right ventricular reverse remodelling after balloon pulmonary angioplasty. Eur Respir J 2014;43(5):1394-1402. doi:10.1183/09031936.00012914

18. Zoppellaro G, Badawy MR, Squizzato A, et al. Balloon Pulmonary Angioplasty in Patients With Chronic Thromboembolic Pulmonary Hypertension - A Systematic Review and Meta-Analysis. Circ J 2019;83(8):1660-1667. doi:10.1253/circj.CJ-19-0161

19. Han QJ, Witschey WR, Fang-Yen CM, et al. Altered Right Ventricular Kinetic Energy Work Density and Viscous Energy Dissipation in Patients with Pulmonary Arterial Hypertension: A Pilot Study Using 4D Flow MRI. PLoS One 2015;10(9):e0138365. Published 2015 Sep 29. doi:10.1371/journal.pone.0138365

20. Odagiri K, Inui N, Hakamata A, et al. Non-invasive evaluation of pulmonary arterial blood flow and wall shear stress in pulmonary arterial hypertension with 3D phase contrast magnetic resonance imaging. Springerplus 2016;5(1):1071.

Published 2016 Jul 13. doi:10.1186/s40064-016-2755-7

21. Ramos JG, Fyrdahl A, Wieslander B, et al. Cardiovascular magnetic resonance 4D flow analysis has a higher diagnostic yield than Doppler echocardiography for detecting increased pulmonary artery pressure. BMC Med Imaging 2020;20(1):28. Published 2020 Mar 6. doi:10.1186/s12880-020-00428-9

22. Spurk J, Aksel N, Fluid Mechanics second edition 2008, Springer, DOI 10.1007/978-3-540-73537-3

23. O'Brien KR, Cowan BR, Jain M, Stewart RA, Kerr AJ, Young AA. MRI phase contrast velocity and flow errors in turbulent stenotic jets. J Magn Reson Imaging 2008;28(1):210-218. doi:10.1002/jmri.21395

Figure titles and legends

Figure 1. Assessment of blood flow in the pulmonary artery (PA). Planes were set at the inlets of the pulmonary trunk and right and left main PAs to evaluate volume flow rate (VFR). Moreover, 30 planes were set in the pulmonary trunk along the centerline to evaluate net VFR and secondary flow in each plane. The centerline of the PAs was defined as the normal direction of the plane. The duration of the vortical flow (the length of cardiac phases with vortex present) was quantified as the full width at half maximum (FWHM) of the peak of the time course of VFR of backward flow ($\overline{\mathrm{VFR_b}}$). The size of vortical flow was evaluated as the proportion of the area of the backward flow present in each cross-section, and the time-averaged area ratio was defined by $\overline{\text{area ratio}} = \sum^{N_\mathrm{p}} A_\mathrm{b}/A/N_\mathrm{p}$, where A_b is the cross-sectional area occupied by the backward flow, A is the entire cross-sectional area, and N_p is the number of data acquisition phases of four-dimensional-flow magnetic resonance imaging (i.e., time resolution 14–24 phases/cardiac cycle). The velocity, $\boldsymbol{v}$, in a cross-sectional plane may be either forward or backward ($v_\mathrm{n,f}$ and $v_\mathrm{n,b}$, respectively), as shown in Fig. 1. The mean backward flow rate during a cardiac cycle is $\overline{\mathrm{VFR_b}} = \sum^{N_\mathrm{p}} \mathrm{VFR_b}/N_\mathrm{p} = \sum^{N_\mathrm{p}} \int |v_{n,\mathrm{b}}| A_\mathrm{b}/N_\mathrm{p}$, where $v_\mathrm{n,b}$ is the normal component of the spatially averaged

449 backward flow velocity.

450

451 **Figure 2.** Perioperative changes in the full width at half maximum (FWHM) of the peak
452 of the time course of volume flow rate of backward flow ($\overline{\mathrm{VFR_b}}$), area ratio between the
453 cross-sectional area occupied by the backward flow (A_b) and the entire cross-sectional
454 area (A), and the time-averaged $\overline{\mathrm{VFR_b}}$ during a cardiac cycle.

455

456 **Figure 3**. Perioperative changes in the full width at half maximum (FWHM) of the peak
457 of the time course of the volume flow rate of backward flow ($\overline{\mathrm{VFR_b}}$), area ratio between
458 the cross-sectional area occupied by the backward flow (A_b) and the entire
459 cross-sectional area (A), and time-averaged $\overline{\mathrm{VFR_b}}$ for two groups in reference to the
460 median decrease in mean pulmonary artery pressure, $\Delta P = 14$ [mmHg]: the large ($\Delta P \geq$
461 14 [mmHg], 15 cases) and small ($\Delta P < 14$ [mmHg], 13 cases) decrease groups.

462

463 **Figure 4**. Perioperative changes in the volume flow rate (VFR) at the inlets of the (A)
464 the pulmonary trunk, and (B) right, and (C) left main pulmonary arteries (PAs).

465

466 **Figure 5**. Flow streamlines in late systole of two patients; one each from the large ($\Delta P \geq$

14 [mmHg]) ((A) before and (B) after BPA) and small ($\Delta P < 14$ [mmHg]) decrease groups ((C) before and (D) after BPA).

Figure 6. Isosurface plots of the helicity density (H_d) and second invariant of the velocity gradient tensor (Q) during late systole in the same patients as those displayed in Fig. 5. The plots of H_d and Q are shown in (A) before and (B) after BPA for the patient in the large decrease group, and (C) before and (D) after BPA for the one in the small decrease group, respectively. ΔP: decrease in mean pulmonary artery pressure.

Tables

Table 1: Right heart catheterization data before and after balloon pulmonary angioplasty (BPA). Patients were classified into two groups with reference to the median ΔP of 14 [mmHg]: the large (ΔP ≥ 14 [mmHg], 15 cases) and small (ΔP < 14 [mmHg], 13 cases) decrease groups. PAP: pulmonary artery pressure, PVR: pulmonary vascular resistance, RVEF: right ventricular ejection fraction, RVCI: right ventricular cardiac index, ΔP: decrease in mean pulmonary artery pressure.

Figures

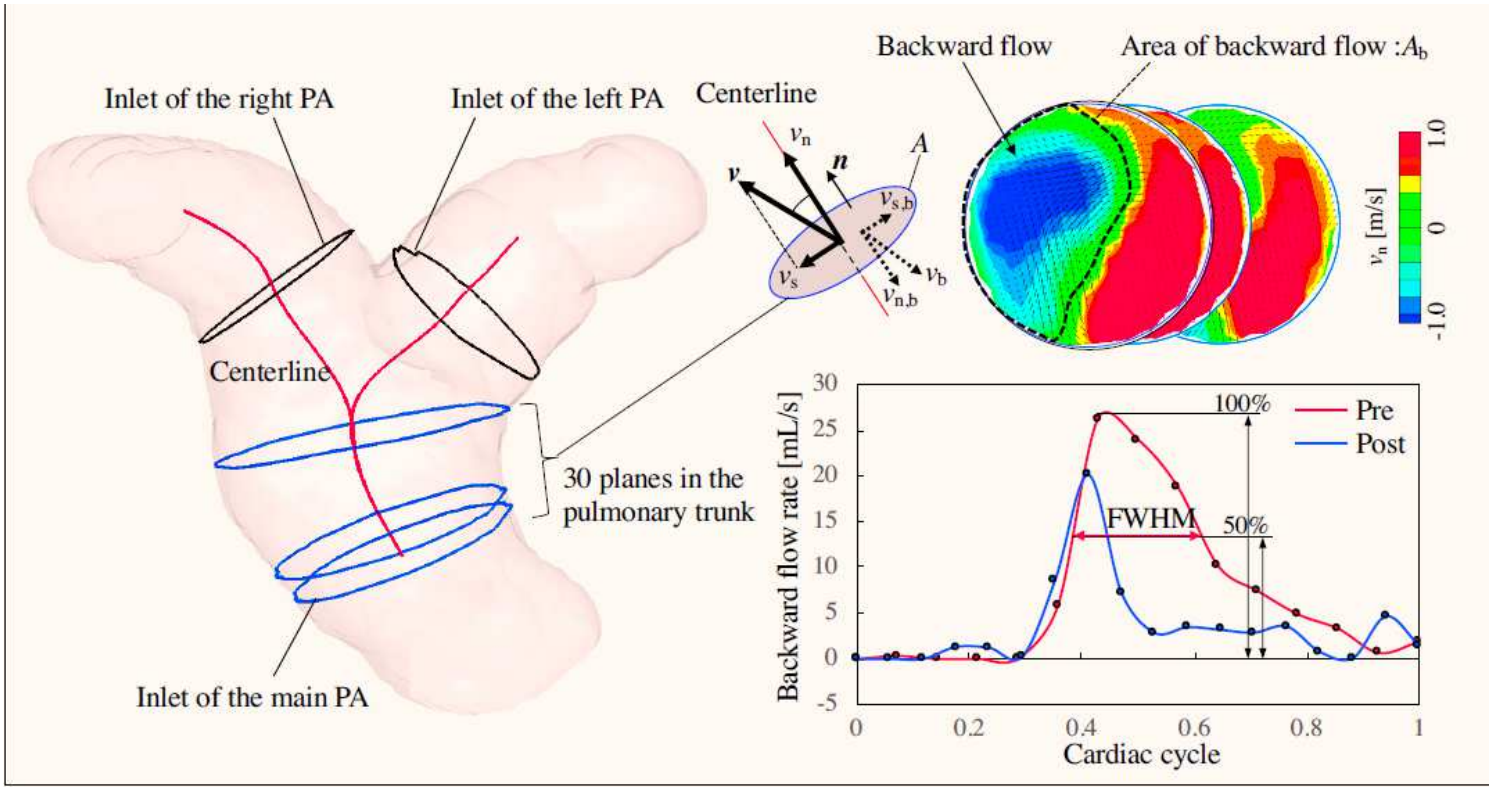

Figure 1

See the Manuscript Files section for the complete figure caption.

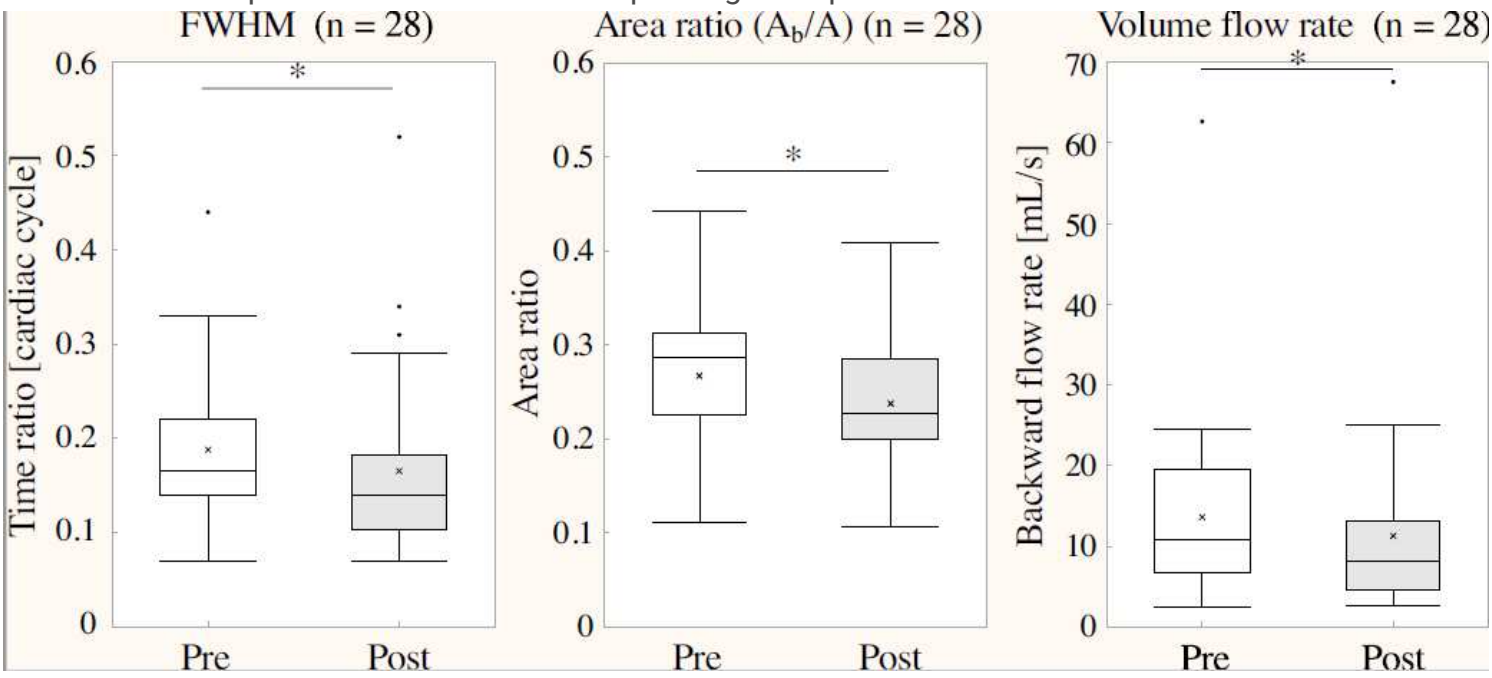

Figure 2

See the Manuscript Files section for the complete figure caption.

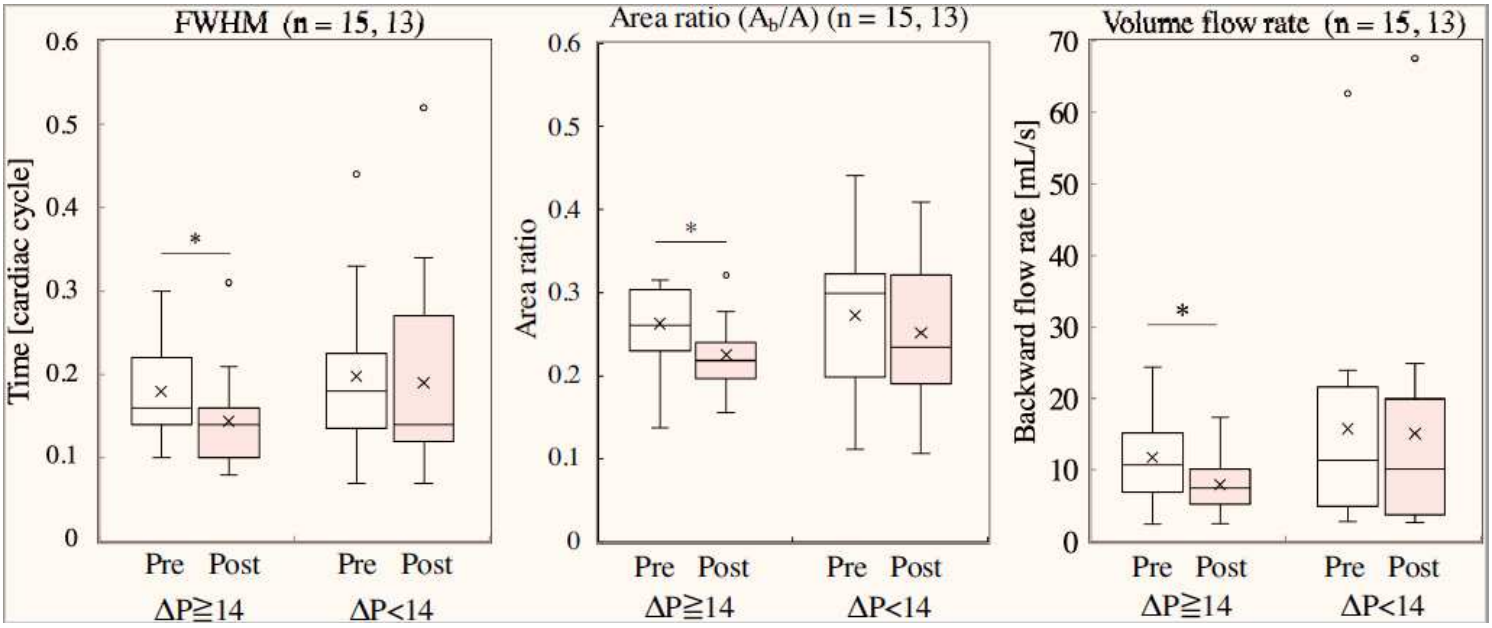

Figure 3

See the Manuscript Files section for the complete figure caption.

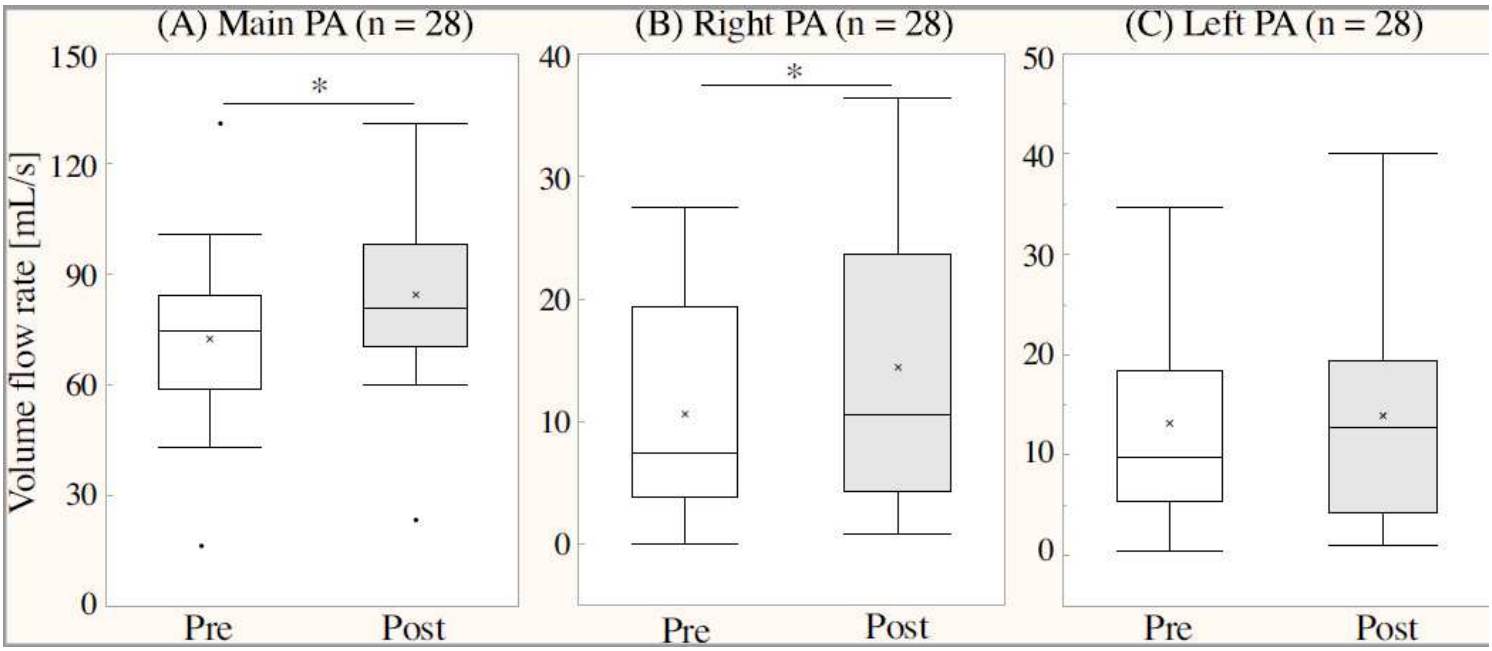

Figure 4

See the Manuscript Files section for the complete figure caption.

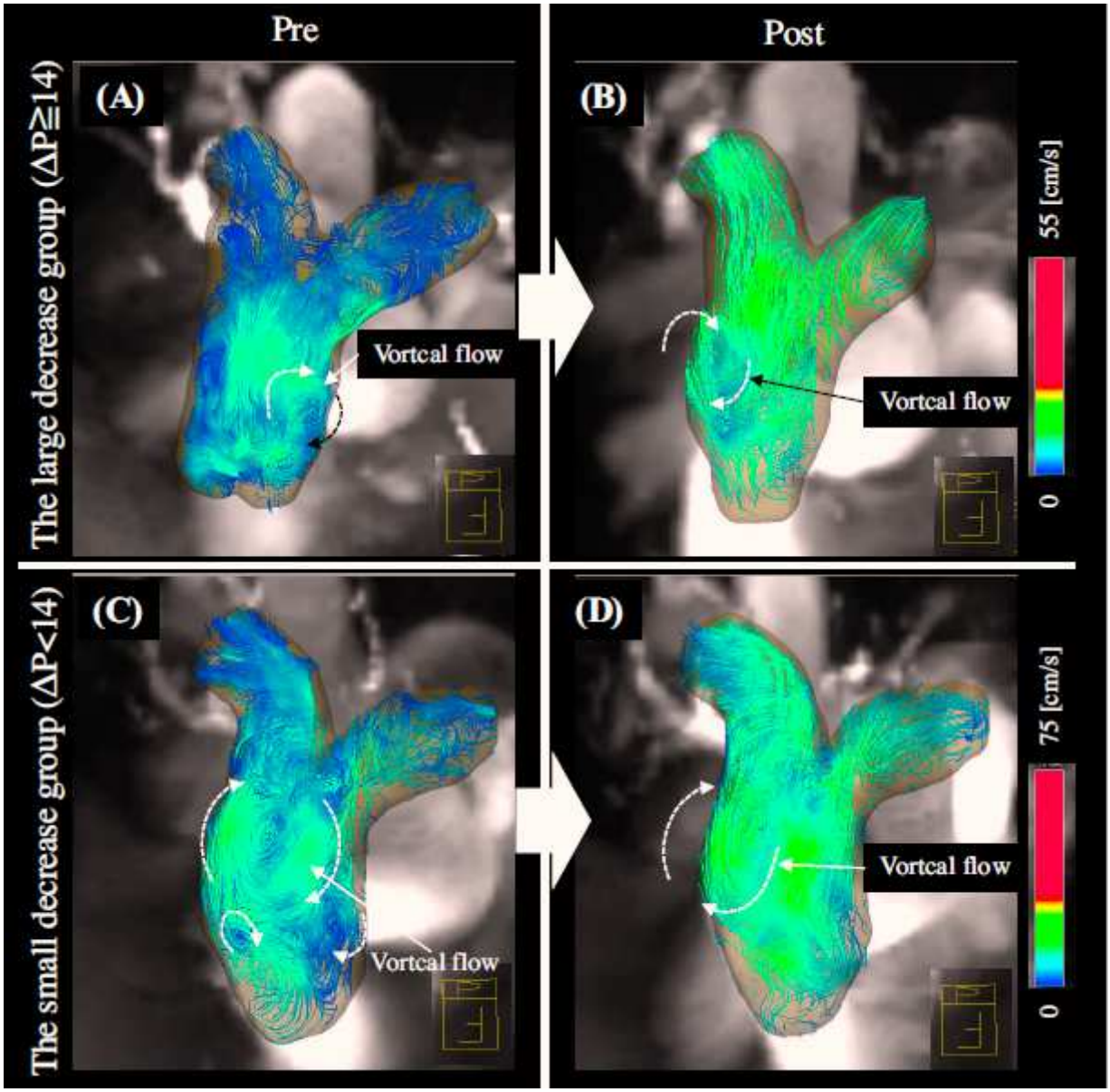

Figure 5

See the Manuscript Files section for the complete figure caption.

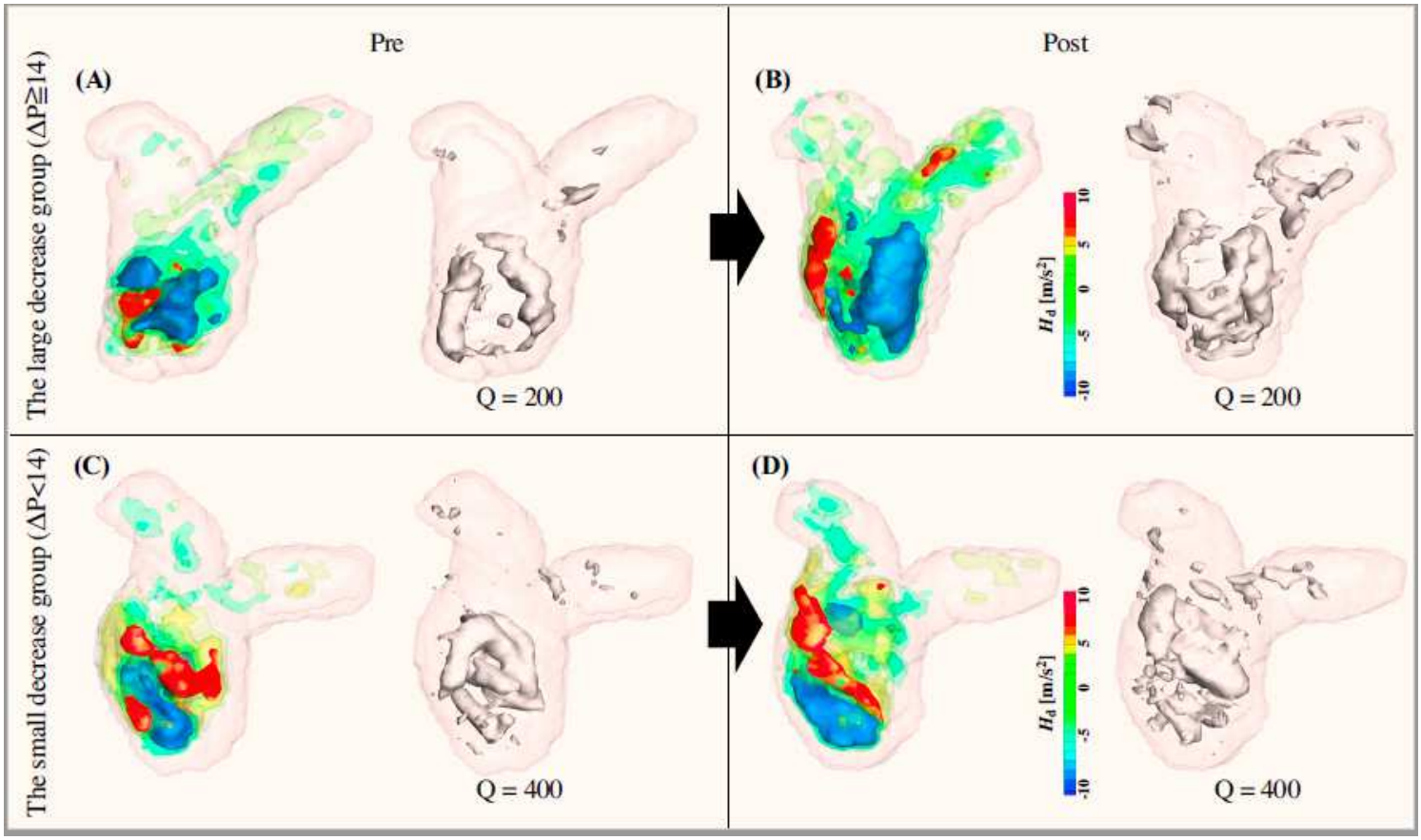

Figure 6

See the Manuscript Files section for the complete figure caption.

Supplementary Files

This is a list of supplementary files associated with this preprint. Click to download.

- Table1.eps